Assessing the importance of spatio-temporal RCM resolution when estimating sub-daily extreme precipitation under current and future climate conditions

Sunyer Pinya, Maria Antonia; Luchner, J.; Onof, C.; Madsen, H.; Arnbjerg-Nielsen, Karsten

Published in:
International Journal of Climatology

Link to article, DOI:
10.1002/joc.4733

Publication date:
2017

Document Version
Peer reviewed version

Assessing the importance of spatio-temporal RCM resolution when estimating sub-daily extreme precipitation under current and future climate conditions

Short title: Sub-daily extreme precipitation from RCMs

M.A. Sunyer, Department of Environmental Engineering, Technical University of Denmark, Lyngby, Denmark. Now at Arup, London, United Kingdom. Maria.sunyer-pinya@arup.com, +44 20 7755 5032.

J. Luchner, DHI, Hørsholm, Denmark

C. Onof, Imperial College London, London, United Kingdom

H. Madsen, DHI, Hørsholm, Denmark

K. Arnbjerg-Nielsen, Department of Environmental Engineering, Technical University of Denmark, Lyngby, Denmark.

Abstract

The increase in extreme precipitation is likely to be one of the most significant impacts of climate change in cities due to increased pluvial flood risk. Hence, reliable information on changes in sub-daily extreme precipitation is needed for robust adaptation strategies.

This study explores extreme precipitation over Denmark generated by the regional climate model (RCM) HIRHAM-ECEARTH at different spatial resolutions (8, 12, 25 and 50 km), three RCM from the RiskChange project at 8 km resolution and three RCMs from ENSEMBLES at 25 km resolution at temporal aggregations from 1 h to 48 h. The performance of the RCM simulations in current climate as well as projected changes for 2081–2100 are evaluated for non-central moments of order 1 to 3 and for the 2 and 10 year event.

The comparison of the RCM simulations and observations shows that the higher spatial resolution simulations (8 and 12 km) are more consistent across all temporal aggregations in the representation of high order moments and extreme precipitation. The biases in the spatial pattern of extreme precipitation change across temporal and spatial resolution. The hourly extreme value distributions of the HIRHAM-ECEARTH simulations are more skewed than the observational dataset, which leads to an overestimation by the higher spatial resolution simulations. Nevertheless, in general, under current conditions RCM simulations at high spatial resolution represent extreme events and high order moments better.

The changes projected by the RCM simulations depend on the GCM-RCM combination, spatial resolution and temporal aggregation. The simulations disagree on the magnitude and spatial pattern of the changes. However, there is an agreement on higher changes for lower temporal aggregation and higher spatial resolution.

Overall, the results from this study show the influence of the spatial resolution on the precipitation outputs from RCMs. The biases of the RCM simulations increase and the projected changes decrease for decreasing spatial resolution of the simulations. This points towards the need for high spatial and temporal resolution RCMs to obtain reliable information on changes in sub-daily extreme precipitation.

Key words: RCM, extreme precipitation, high spatial resolution, high temporal resolution, performance, future changes

1. Introduction

The recent special report from the Intergovernmental Panel on Climate Change (IPCC) on the effects of climate change on extreme events showed that extreme precipitation is expected to increase in Northern Europe (IPCC, 2012). This is in agreement with the findings from several previous studies, e.g. Boberg *et al.* (2010), Christensen and Christensen (2003), and Fowler *et al.* (2007). The increase in extreme precipitation is expected to be one of the most critical impacts of climate change in cities (Fowler and Hennessy, 1995; IPCC, 2012). Thus, the design of robust adaptation strategies requires reliable information on changes in extreme precipitation.

Information on changes in extreme precipitation at high spatial and temporal resolution is especially important in urban hydrological applications. These changes are commonly estimated from a combination of dynamically and statistically downscaled global climate models (GCMs). Dynamical downscaling is performed by nesting high-resolution models within a sub-region of a GCM (e.g. Europe, Scandinavia). Usually these models are referred to as regional climate models (RCMs) and have a higher spatial resolution than the GCMs, typically between 10 and 50 km. Statistical downscaling methods are often used to further downscale RCMs. These methods are based on statistical techniques which aim at reducing the bias of the RCMs and producing precipitation estimates with high spatial and temporal resolution. See Maraun *et al*. (2010) for a review and discussion of statistical downscaling methods and Giorgi and Gutowski (2015) for more information on dynamical downscaling.

In the last decade, large datasets of RCMs covering Europe have been made available. The ENSEMBLES project (van der Linden and Mitchell, 2009) provided a large ensemble of RCM outputs at spatial resolutions of 25 and 50 km and at daily temporal resolution. The RCM outputs recently made publically available from EURO-CORDEX (Jacob *et al.*, 2013, Giorgi and Gutowski,

2015) have spatial resolutions of 0.11º and 0.44 º (around 12 and 50 km, respectively) and temporal aggregation of 3 h, one day, one month and one season. Currently, only few RCMs are publically available at 3 h aggregation. The RCMs at a spatial resolution of 12 km from EURO-CORDEX are more suitable for the needs in urban hydrological applications than the RCMs at a coarser spatial resolution from previous projects. Nonetheless, the daily aggregation of most RCMs available from EURO-CORDEX is still too coarse to allow a proper analysis of urban water management options (Schilling, 1991; Arnbjerg-Nielsen *et al.*, 2013).

According to Chan *et al.* (2014a), RCMs with spatial resolution of the order 10^1 km are in the so called "grey zone". This term is used to refer to the spatial resolutions at which the assumptions in the convective parameterisation become invalid (Chan *et al.*, 2014a; Westra *et al.*, 2014; Yu and Lee, 2010). For these spatial resolutions, the area of convection cannot be considered small compared to the spatial resolution of the RCM (Westra *et al.*, 2014) and, therefore, it is not possible to properly represent convective precipitation in a parameterised form (Chan *et al.*, 2014a; Chan *et al.*, 2014b). However, research on improving the parametrization is ongoing. Grell and Freitas (2014) presented a convective parametrization approach which is tested using non-hydrostatic mesoscale models with spatial resolutions ranging from 5 to 20 km.

The RCMs in the "grey zone" might lead to unrealistic extreme precipitation. Chan *et al.* (2014a, 2014b) obtained physically implausible extreme precipitation from the RCM at 12 km resolution, which they argued was due to this model being in the "grey zone".

Currently, large ensembles of RCMs similar to the ones in EURO-CORDEX or ENSEMBLES at both high spatial and temporal resolutions are not publically available. Only a few RCM outputs are available at sub-daily temporal aggregation (often at hourly aggregation). A total of four RCMs from the RiskChange project (Fox Maule *et al.*, 2014, Mayer *et al.*, 2015) covering most of

Scandinavia are now available at a spatial resolution of approximately 8 km and hourly temporal aggregation. The lack of large ensembles of RCMs at sub-daily resolution is mainly due to storage capacity required to save these results from the simulation runs. Additionally, RCMs have often been considered to perform worse at hourly than at daily aggregation (e.g. Gregersen *et al.*, 2013; Hanel and Buishand, 2010; Maraun *et al.*, 2010).

Some recent studies point towards the fact that the representation of sub-daily extreme precipitation in RCMs improves with increasing spatial resolution. Prein *et al.* (2015a) includes a comparison of the precipitation outputs from the EURO-CORDEX RCMs at spatial resolutions of 0.11º and 0.44º for several European regions. They found that in most cases the 0.11º simulations tend to produce heavier 3 h and daily extreme precipitations than simulations at 0.44º resolution. In some cases, the extreme precipitation estimates of the 0.11º simulations lead to a larger bias compared to the 0.44º simulations. They also found that, in general, the simulations at 0.11º resolution presented larger improvements in the representation of extreme precipitation (except for winter) for 3 h than for daily temporal aggregation. Prein *et al.* (2015a) also compared the proportion of convective precipitation in the EURO-CORDEX simulations and found no major difference during winter between the two resolutions but that during summer the 0.11º runs tend to reduce the proportion of convective precipitation (i.e. more precipitation is explicitly generated by the model dynamics).

Chan *et al.* (2014) and Kendon *et al.* (2014) compared the errors and the differences in the changes projected by the same RCM at two different spatial resolutions (a convective permitting RCM at 1.5 km and a RCM at 12 km using convective parameterization). They concluded that the convective permitting RCM is more suitable to represent small scale sub-daily extreme precipitation than the RCM at lower spatial resolution. In addition, the convective permitting RCM showed larger changes in high intensities for short durations when compared to the coarser resolution RCM. Ban

et al. (2014) evaluated the precipitation outputs from a convective permitting model at a resolution of 2.2 km and a model at 12 km where convective precipitation was parametrised on an extended Alpine domain. They found that the convective permitting model improved considerably both daily statistics and hourly extreme events, with larger improvements at hourly temporal aggregation. Fosser *et al*. (2014) found similar results to Ban et al. (2014) in a study assessing a convective permitting model at 2.8 km resolution and a model at 7 km resolution using convective parameterisation over Germany. Prein *et al*. (2013a and 2013b) also found a similar added value of the convective permitting simulations. Prein *et al.* (2013b) concluded that if the main interest is in large scale average heavy precipitation both the convective permitting (4 km resolution) and the models with convective parameterisation (12 and 36 km resolution) are sufficient for all seasons, except summer. In summer the representation of heavy precipitation is significantly improved in the 4 km simulation. Similarly to Kendon *et al*. (2014), Ban *et al*. (2015) compared extreme precipitation over Switzerland using the same models as Ban *et al*. (2014). They found that the convective permitting model improved the representation of extreme precipitation. Both models lead to similar changes in the intensity of daily and hourly extreme precipitation, except for the very high percentiles (larger than 99.9%) where the model at 12 km leads to higher changes. They concluded that their results suggest that both daily and hourly increases in extreme precipitation are consistent with the Clausius-Clapeyron scaling. Prein *et al.* (2015b) provided a thorough review of convective permitting models and stated the need for coordinated modelling programs to assess the full potential of these models.

Tripathi and Dominguez (2013) compared the representation of 3 h precipitation of the same RCM at 10 and 50 km spatial resolution (both simulations used the same convective parameterisation). They found that the bias of the RCM at 10 km resolution of summer mean precipitation was higher than that of the RCM at a coarser resolution, but that it performed better in representing extreme

precipitation in summer. The models performed equally in the representation of mean and extreme precipitation in winter. A recent study by Zheng *et al*. (2015) compared changes in observed annual maximum precipitation at different temporal aggregations in Sydney. They found smaller increases in extreme precipitation for larger temporal aggregations. In fact they found a decrease in extreme precipitation for temporal aggregations larger than 3 h. They explained that the different changes for different temporal aggregations were due to the season in which the annual maximum event takes place (i.e. most sub-daily extremes take place in summer while larger duration events tend to take place in autumn and winter).

Westra *et al.* (2014) reviewed the advances and remaining challenges in the representation of future changes in sub-daily extreme precipitation. They pointed out the need for assessing which spatial resolution of RCMs is needed to have confidence in extreme precipitation projections.

This study analyses outputs from the same RCM at different temporal aggregation (1 to 48 h) and spatial resolution (8 to 50 km) over Denmark as well as outputs from three additional models at 8 km resolution and three models at 25 km resolution. Both the performance and the changes projected by the RCM simulations on a range of precipitation characteristics and extreme precipitation are analysed. The main goal of this study is to analyse whether there is a relation between the spatial resolution of the RCM and its performance as well as the changes projected at different temporal aggregations. The study aims to contribute to the research question of which spatio-temporal resolution is needed of RCMs to obtain reliable information on changes in sub-daily extreme precipitation.

2. Data

2.1. Observations

Precipitation data from a network of high-resolution RIMCO tipping bucket rain gauges operated by the Water Pollution Committee of the Society of Danish Engineers and the Danish Meteorological Institute (DMI), usually referred to as the SVK network, is the main observational dataset used in this study (Jørgensen *et al.*, 1998). This network was primarily designed for measuring high intensity precipitation events over urban areas which is why a rather high threshold for dry weather is applied, i.e. hours with less than approximately 0.2–0.4 mm of rain are considered dry (Jørgensen *et al.*, 1998). While this dry weather threshold does not affect extreme event calculations, it affects results for statistical moments and temporal aggregation.

For this study, the available data consists of precipitation intensity at the temporal aggregations 1, 3, 6, 12, 24, and 48 h. The stations with data covering the time period from 1991 to 2010 which have less than 10% of data missing have been used in the study. This corresponds to a total of 40 stations of which 15 are located in the Copenhagen area (Eastern part of Zealand) (see Figure 1).

The observational dataset Climate Grid Denmark (CGD) is also used in this study for further comparison of the RCM and SVK data. The CGD dataset is a gridded precipitation product from DMI based on interpolation of more than 300 HELLMAN gauges covering Denmark (Scharling, 2012). It provides daily precipitation data at a spatial resolution of 10 km (see Figure 1) for the time period 1989 – 2010, the time period 1991 – 2010 is used here.

2.2. Regional climate models

Four simulations of the RCM HIRHAM version 5 driven by the GCM ECEARTH at 8, 12, 25, and 50 km spatial resolution (hereby referred to as HE8, HE12, HE25, HE50, respectively) have been

considered in this study. From these models, precipitation output is available at 1 h aggregation. For this study, the data is aggregated to precipitation intensity at 1, 3, 6, 12, 24, and 48 hours. The outputs from HE12 and HE50 are from the same model run as the outputs made publically available in EURO-CORDEX. HE8 and HE25 were made available through the RiskChange project (http://riskchange.dhigroup.com) and the Centre for Regional Change in the Earth System (CRES) (http://cres-centre.net), respectively. HE8 has a different spatial domain than HE12, HE25 and HE50. It covers most of Scandinavia (Mayer *et al.*, 2015) while HE12, HE25 and HE50 cover Europe.

The HIRHAM version 5 is a hydrostatic RCM that combines the dynamics from the short-range weather forecasting system HIRLAM-7 with the physical parameterisation of ECHAM5 (Christensen *et al.*, 2007). Vertical acceleration and hence sound waves are ignored in the hydrostatic assumptions. Hence, these models have a limited capability to represent small scale phenomena such as extreme precipitation due to convection or orographic uplift. For details on the dynamics and the physical parameterisation of HIRHAM5 the reader is referred to Unden *et al.* (2002) and Roeckner *et al.* (2003), respectively. The ECEARTH model, which was developed as part of a Europe-wide consortium, is a recent earth system model which builds on model technology from the European Centre for Medium Range Weather Forecasting (ECMWF). For a detailed model description the reader is referred to Brandt (2010).

For HE12 and HE50 both the time series for convective and the large scale precipitation have been made available for this study by DMI. These time series have been used to compare the relevance of the convective precipitation in the outputs of these two simulations.

In order to compare the results obtained from the HIRHAM-ECEARTH simulations the study also includes six additional RCM outputs available at 1 h temporal aggregation over Denmark. These are

three simulations from the RiskChange project at 8 km spatial resolution and three RCMs at a spatial resolution of 25 km from the ENSEMBLES project. The three RCMs from RiskChange are: the WRF RCM driven by ECEARTH, WRF driven by NorESM, and the HIRHAM RCM driven by NorESM, hereby referred to as WE8, WN8 and HN8, respectively. A more detailed description of these three models and HE8 can be found in Fox Maule *et al.* (2014) and Mayer *et al.* (2015) . The three additional RCMs from ENSEMBLES used are HIRHAM driven by ECHAM5, HIRHAM driven by BCM and RACMO driven by ECHAM5, hereby referred to as HEc25, HB25 and REc25. See more details on the ENSEMBLES models in van der Linden and Mitchell (2009). The computaitonal domain of all the RiskChange simulations is shown in Mayer *et al.* (2015), the domain of the ENSEMBLES simulations is shown in van der Linden and Mitchell (2009), and the domain of the EURO-CORDEX simulations is shown in Prein *et al.* (2015a).

It should be noted that HE8, WE8, WN8, HN8 and HE12 are in the so called "grey zone" (considered here as resolutions of the order of 10^1 km as discussed in Chan *et al.* (2014a)).

All RCM simulations are driven by the representative concentration pathways (RCP) 4.5 and 8.5 (Moss *et al.*, 2010), except HEc25, HB25 and REc25 which are driven by the SRES emission scenario A1B (Nakićenović *et al.*, 2000). Here we consider only the results of RCP 4.5, i.e. the outputs from HEc25, HB25 and REc25 are not considered in the assessment of changes from current to future periods. The time periods used to represent current and future climate are 1991–2010 and 2081–2100, respectively. It should be noted that RCM outputs for current climate are available only up to 2005 and the results from RCP 4.5 are used from 2006 to 2010. The spatial domain of the RCM selected for this study is all the land grid points covering Denmark (see Figure 1). For the HE8 model, these were selected from the land sea mask choosing grid cells with a land content greater or equal to 0.4. The land sea mask was not available for all models. For these

models the land grid cells were selected by visual inspection, which should be sufficient for the purpose of this study, the precise selection of land grids should be based on the land-sea mask.

A threshold for dry hours of 0.1 mm/h has been applied to all the RCM data in order to address the drizzling issue known for most RCMs (Kjellström *et al.*, 2010). All the values lower or equal than this threshold are set to 0 mm/h. This threshold has been used in previous studies (e.g. Kendon *et al.*, 2014; Willems and Vrac, 2012).

FIGURE 1

3. Methodology

The performance of the RCM simulations is evaluated using a set of precipitation properties ranging from large scale properties such as mean precipitation to local scale precipitation properties such as extreme precipitation. The temporal aggregation covers the range 1 – 48 h. For all temporal aggregations, grid points and SVK stations over Denmark, the following properties are included in the assessment of performance:

- Areal average non-central moments of order 1 to 3 for winter (December-January-February) and summer (June-July-August)
- Areal average and spatial patterns of Intensity-Duration-Frequency (IDF) curves for 2 and 10 years return periods, and parameters of extreme value distributions.
- Spatial pattern of mean annual precipitation.

The changes from present to future are estimated for the same precipitation properties. These changes, referred to as change factors (CF), are estimated from the RCM outputs as the ratio between future and present. CFs are estimated separately for each temporal aggregation and grid point in the RCM.

3.1. Non-central moments of order 1 to 3 for winter and summer

The non-central moments of order 1 to 3 at different temporal aggregations are estimated to assess the temporal scaling behaviour of precipitation. This refers to the fact that a log-log linear relationship is generally found to exist over a range of temporal scales of non-central moments. This relationship is often used in precipitation disaggregation methodologies (e.g. Gupta and Waymire, 1993; Molnar and Burlando, 2005; Onof and Arnbjerg-Nielsen, 2009; Over and Gupta, 1996). Previous studies have shown that a single log-log linear relationship can be used to downscale from daily to hourly precipitation. However, it must be noted that this relationship may not hold for sub-hourly precipitation. Nguyen *et al.* (2007) showed that there is a shift in the scaling properties of precipitation at a temporal resolution of approximately 40min.

The non-central moments of order q, for q equal to 1, 2, and 3, are estimated for each temporal aggregation (1, 3, 6, 12, 24 and 48 h). These temporal aggregations are expressed using a temporal scale, λ, which is defined as 2^{-n}, where n refers to the level of the temporal aggregation in the cascade model (Molnar and Burlando, 2005) often used to describe the temporal scaling behaviour of precipitation, n equal to 0 corresponds to the temporal aggregation of 48 h, n equal to 1 to 24 h and so on. The level of 1 h is obtained through linear interpolation between the level 5 (1.5 h) and 6 (0.75 h), which leads to n equal to 5.667. For example, $\log(\lambda)$ for 48 h is 0 and $\log(\lambda)$ of 1h is -1.706. The non-central moment of order q for the temporal aggregation i, $M_i(q)$, is the expected value of $(X_i)^q$, where X_i is the precipitation at the temporal aggregation t (Molnar and Burlando, 2005):

$$M_t(q) = E[{X_t}^q] \quad (1)$$

In an attempt to avoid the issues arising from comparing point measurements (SVK) and gridded data (RCM and CGD) (see e.g. Chen and Knutson, 2008; Sunyer *et al.*, 2013), the non-central

moments of order 2 and 3 have been standardised using the moment of order 1 to obtain scale independent estimates. The standardised moments have been estimated as $\frac{M_t(q)}{M_t(1)^q}$. This approach uses the assumption that a proportional relationship exists between precipitation at different spatial scales as suggested by Areal Reduction Factors (ARF) (Wilson, 1990).

ARFs are simple empirically based factors, which depend on the temporal and spatial resolution and are often used to obtain estimates of areal precipitation (see more detailed description in 3.2 and Table 1). We are not aware of ARF being used directly on moments. Hence, the use of standardised moments has been used in an attempt to obtain spatial scale independent estimates.

3.2. Extreme value analysis

Extreme precipitation intensities are calculated corresponding to 2 and 10 year return periods. The extreme value series are extracted from the time series using a Partial Duration Series (PDS) methodology, where an average of 3 events per year is applied to select the extreme values. An independence criterion based on the inter-event time between extremes is used to ensure that the events included in the extreme value series are independent. Only events separated by a no-rain period of at least the considered duration are included. The precipitation intensity is estimated by fitting a Generalised Pareto Distribution (GPD) to the extreme value series using the L-moments approach suggested by Hosking and Wallis (1993). As shown in previous studies (Madsen *et al.*, 2002; Madsen *et al.*, 2009), the shape parameter in the GPD can be assumed to be homogenous over Denmark. The regional shape parameter, $k_{REG,}$ and the resulting relationship for the T-year event for one grid cell or station, x_T, are estimated as:

$$L_{CV,REG} = \frac{1}{M}\sum_{i=1}^{M} L_{CV,i}$$

$$k_{REG} = \frac{1}{L_{CV,REG}} - 2 \qquad (2)$$

$$x_T = x_0 + (\mu_x - x_0)\frac{1+k_{REG}}{k_{REG}}\left[1-\left(\frac{1}{lT}\right)^{k_{REG}}\right]$$

where L_{CV} denotes the L coefficient of variation, M denotes the number of grid cells or number of stations for the SVK dataset, x_0 is the threshold level based on the average number of annual exceedances, l, and μ_x is the average of the extracted extreme value time series.

As for the non-central moments, the T-year events are estimated for all the grid points and stations for the temporal aggregations of 1, 3, 6, 12, 24, and 48 hours.

ARF have been used to be able to compare the results obtained from the gridded datasets (RCM and CGD) with the results from the SVK data. The factors suggested by Wilson (1990), shown in Table 1, have been used here to obtain point estimates from gridded precipitation of the RCM simulations and CGD (i.e. $X_{t,\ point\ estimate} = \mathrm{ARF}_{t,s} \cdot X_{t,s}$, where s represents the spatial resolution and t the temporal aggregaiton) For a more detailed description of the approach used to derive the ARF see Wilson (1990).

TABLE 1

3.3. Spatial pattern

The spatial patterns over Denmark are assessed in terms of the mean annual precipitation and 10 year return period of daily and hourly precipitation. The spatial pattern in the mean annual

precipitation is mainly used to assess whether the difference in model domain between HE8 and the other models has an impact. CGD is used to assess the RCM ability to represent the observed spatial pattern at daily resolution and for mean annual precipitation.

The spatial pattern is analysed using the percent variation from the spatial average of all land grid cells, Δ, which is calculated as:

$$\Delta = \frac{(x_i - x_{avg})}{x_{avg}} * 100 \quad (3)$$

where x_i denotes the value of the land grid cell i and x_{avg} denotes the spatial average over all land grid cells of the respective dataset.

This visualisation method simplifies the comparison of the spatial pattern across different datasets and solves the problem of comparing spatial patterns of datasets with different spatial resolutions and biases.

3.4. Bootstrapping

Bootstrap resampling is used to assess the significance of model biases and future changes in extreme precipitation with respect to year-to-year variability. The approach used here is inspired by the one used in Kendon *et al*. (2014). It includes four steps: (1) sample N years with replacement from the N years of data; (2) estimate the T-year events for each grid point for the N sampled years obtained from step 1; (3) for each T-year event, calculate the average of all the grid points over Denmark; (4) repeat steps 1 to 3 to obtain 1000 estimates of the area averaged T-year event over Denmark.

This bootstrapping procedure is applied to the extreme value series obtained from the observational data and the RCM data for present and future. As in Kendon *et al.* (2014), the bootstrap samples are used to assess whether differences between the observations and the RCM simulations are

significant. This is assessed using the Wilcoxon Rank Sum test, which assesses whether the medians of the two bootstrap samples obtained from two datasets (e.g. one RCM and the SVK data) are equal. The Wilcoxon test is applied instead of the t-test because the bootstrap samples cannot be assumed to be normally distributed.

4. Results and discussion

This section is divided into two main parts. First the performance of the RCM simulations in present climate is investigated; this is followed by the assessment of the CFs. In each part the RCM outputs are analysed with focus on different temporal aggregations and by comparing the spatial pattern.

4.1. RCM performance

4.1.1. Areal average moments of order 1, 2 and 3

Figure 2 shows the relationship between the moments at different temporal aggregations for winter and summer. The moments of order 2 and 3 have been standardised as described in the methodology section.

First we compare the results for the two observational datasets. For both winter and summer the estimated mean (moment of order 1) is larger for CGD than for SVK but the opposite is observed for the standardised moment of order 2 and 3. The difference between SVK and CGD is considerably larger in winter than in summer for all the moments. In winter, the values of CGD for the standardised moments of order 2 and 3 fall outside the range of minimum and maximum value of all SVK stations. For the moment of order 1 and for all the moments in summer the values of CGD fall within the range of values from all the SVK stations.

The difference in the mean for winter might be due to the RIMCO gauges, which are used in the SVK network. This gauge is known to have a significant under-catch of precipitation when temperature is below zero degrees Celsius because heating of the gauge creates a chimney effect (McMillan *et al.*, 2012). A WMO inter-comparison of solid precipitation measurements from rain gauges also stated that the RIMCO gauge is more sensitive to wind than the HELLMAN gauge, the rain gauge used for CGD. This will have the highest impact in autumn and winter (WMO, 1998). The under-catch of the SVK stations might affect the different temporal aggregations differently and must be taken into account in the analysis of the performance of the RCM simulations.

The difference in mean precipitation as well as the larger standardised moments of order 2 and 3 obtained for SVK compared to CGD illustrate the uncertainty in the observations.

FIGURE 2

The performance of the RCMs depends on the season. In winter all the RCM simulations overestimate the mean when compared to both SVK and CGD. Nonetheless, it should be noted that this might partly be caused by the under-catch of the observational datasets, which is particularly relevant in the SVK stations for winter. The same is observed in summer except for HE8, WE8, HEc25 and HB25, which underestimate the mean. In winter, the RCM simulations underestimate the standardised moments of order 2 and 3 at all temporal aggregations when compared to both SVK and CGD, except HE8 which leads to similar values as CGD. In summer, HE8 and HN8 overestimate and all other RCM simulations underestimate the standardised moments, the differences being more pronounced at low temporal aggregations. In both winter and summer HE8 leads to larger standardised moments than HE12, which in turn leads to larger values than HE25 and HE50.

Similarly to the results described for HE, the three ENSEMBLE RCMs at 25 km resolution (HEc25, HB25 and REc25) underestimate the standardised moments of order 2 and 3 at all temporal aggregations, especially HEc25 and REc25 in summer. As for HE, the underestimation of the standardised moments of order 2 and 3 is more pronounced in summer at low temporal aggregations. The three RCMs at 8 km resolution (HN8, WN8 and WE8) overestimate the mean and underestimate the standardised moments of order 2 and 3 at all temporal aggregations in winter. In summer, the results vary from over- to underestimation. WN8 overestimates the mean while HN8 and WE8 underestimate it. On the other hand, HN8 overestimates the moments of order 2 and 3 and the other two RCMs underestimate it. Overall, the variability of RCM results with the same spatial resolution and the variability of HE simulations at different spatial resolutions is in a similar order of magnitude.

A relevant aspect to be discussed from Figure 2 is whether the RCM simulations and the observations show a similar scaling relation of the moments at different temporal aggregations, i.e. if the lines in Fig. 2 for the standardised moments of order 2 and 3 have similar curvature. For winter all the RCM simulations show a similar scaling relation which is similar to the one obtained from SVK. This may probably be ascribed to the fact that in winter the importance of convective rainfall is low.

In summer, the scaling relations of the RCM simulations differ more than in winter. For both moments the curvature of the RCM simulations deviate more from the curvature of SVK for decreasing spatial resolution. For HE12, HE25 (and HEc25, HB25 and REc25) and HE50 the deviations increase for decreasing temporal aggregation. For both moments, HE8, HN8, WE8 and WN8 have the most similar curvature to the one obtained from SVK. Hence, for the summer season, the variation in short duration precipitation seems to be captured best by the RCM simulations with highest spatial resolution, whereas the variation does not seem to differ

substantially for large durations (24 h and 48 h). For large durations HE12, HE25 and HE50 may then represent present climate best because of a less biased mean value.

4.1.2. Areal average extreme precipitation and spatial pattern of extreme precipitation

The IDF curves in Figure 3 show the influence of the spatial resolution of the RCM in representing short duration extreme events. As in the case of the moments for summer, the differences between large duration (24 and 48h) extreme events simulated by the RCM simulations are small compared to the differences for short durations. For short durations, HE8 lead to higher extreme events and lie outside the bootstrap sample obtained from the observations. For the HE model outputs, in general, HE8 and HE12 overestimate extreme events for all durations while HE25 and HE50 tend to overestimate for large durations and underestimate for short durations. Similarly to the results from Figure 2, HE8 and HE12 show a more consistent error over all durations than HE25 and HE50. As expected, larger differences within the RCM simulations and between the RCM simulations and the observations are obtained for high return periods.

In agreement with the results from HE, the three ENSEMBLE RCMs at 25 km show a larger error in short duration extreme events than in large duration extreme events. For durations larger than 12 h the extreme events simulated for all three RCMs lie within the bootstrap sample obtained from the observations. The results obtained for the three other RiskChange RCMs at 8 km resolution vary considerably. While HE8, HN8 and WN8 overestimate extreme events and lie outside the bootstrap sample (especially for short durations), WE8 tends to underestimate short duration extremes.

FIGURE 3

It should be noted that the results obtained for the two observational datasets are slightly different. CGD leads to slightly lower intensities than SVK (but within the range of values covered by the bootstrap sample). Together with the difference observed for the non-central moments, this

difference between the two observational datasets illustrates the uncertainty in the observations. Nonetheless, it should be noted that in most cases the difference between the observational datasets is smaller than between SVK and the RCM simulations.

The Wilcoxon Rank Sum test of the bootstrap samples show that for all the return periods the IDF curves obtained from the RCM simulations and CGD are significantly different to those obtained from SVK. In addition, all the HE simulations are significantly different to each other except HE8 and HE50 at 24 h aggregation.

The boxplots in Figure 4 compare the magnitude and spatial variation of the 10 year event for 1 h and 24 h temporal aggregations. For 1h, the magnitude and spatial variation increase with increasing spatial resolution of the RCM. Compared to SVK, HE12 and HE25 seem to perform best. HE8, HN8 and WN8 overestimate both the magnitude and the spatial variation. WE8, HEc25, HB25, REc25 and HE50 underestimate the magnitude while HEc25, HB25 and HE50 also underestimate the spatial variation. HB25, REc25 and HE50 largely underestimate and hence cannot be considered suitable for the representation of hourly extreme precipitation over Denmark.

The difference in magnitude and spatial variation between the 8 km models is larger than the difference between the HE models. The difference between the 25 km models is also larger than the variation between the HE models. This result indicates that differences due to spatial resolution are smaller than differences due to different RCM-GCM combinations.

FIGURE 4

The results from Figure 4 also suggest that the physical parameterisation of HIRHAM leads to overestimation of short duration precipitation for spatial resolutions in the so-called grey zone. This is also referred to as “grid-scale storms” and has been discussed in the context of convective permitting simulations (Prein *et al.*, 2015b; Weisman *et al.* 1997). As stated in Prein *et al.* (2015b),

grid-scale storms emerge as convective instability is forced onto an unrealistically coarse scale. This leads to an overestimation of the convective mass flux and precipitation. Weisman *et al*. (1997) looked at the capabilities and limitations of using explicit physics to resolve convection processes. They found that models at a coarser resolution (larger than 4km) are not able to properly represent non-hydrostatic effects.

Kendon *et al.* (2014) found that a convective-permitting RCM represents sub-daily extreme precipitation better than the same RCM at 12 km spatial resolution using convective parameterisation. In line with the findings from Kendon *et al*. (2014), our results point towards the fact that convective permitting high resolution RCM outputs might be needed for the analysis of high temporal resolution extreme events, or convective parameterisations which are adjusted for spatial resolutions in the so-called grey zone.

For 24h, the SVK dataset shows a slightly higher median and a higher spatial variation than the CGD dataset. All RCM simulations except from WE8, HB8 and REc25 tend to overestimate the magnitude of extreme precipitation. There is not a clear relation with respect to the spatial resolution and model performance considering the magnitude and spatial variation. HE8 and HN8 show the largest spatial variation which is similar to the spatial variation seen from the SVK dataset. The differences between the simulations at 8 km resolution and the simulations at 25 km resolution are larger than within the HE simulations. The differences between the HE simulations are relatively small when compared to other RCM outputs. Hence, the performance of the RCM with respect to daily precipitation extremes seems to be less sensitive to the spatial resolution compared to hourly precipitation extremes.

Prein *et al*. (2015a) found that the EURO-CORDEX models at 12 km resolution tend to produce higher daily extreme precipitation than the models at 50 km resolution, but that this cannot be

generalized for all the models, regions and seasons. For 3 h precipitation in Switzerland, they also found that the models at 12 km lead to higher extreme precipitation values than the models at 50 km. The improvements from the 12 km model were found to be larger at 3 h than at 24 h. Similarly to the results found in Prein *et al*. (2015a), we have found that HE12 leads to higher extremes than HE50 for Denmark and that this leads to an improvement of the representation of hourly extremes.

Figure 5 compares the mean extreme value, μ_x, and the shape parameter, k, of the GPD fit to the output of the different RCM simulations and observations. The parameters of the extreme value distribution can explain the results shown in the boxplots in Figure 4 for HE. The outputs from the other six RCM simulations are not included in Fig. 5 to focus only on effects from differences in spatial resolution on the extreme value distribution.

For hourly extreme precipitation, the histograms of μ_x and k of the four RCM simulations differ in their form compared to the SVK data. The two high resolution RCM simulations, HE8 and HE12, show the largest spread in μ_x which explain the larger spreads in the 10 year events. HE12 reproduces well the area average of μ_x and HE8 overestimates it. HE25 and HE50 underestimate the area average of μ_x compared to the SVK data.

The distributions of k show a different relation between the outputs of the simulations than μ_x. HE8, HE12 and HE25 show almost identical regional shape parameters and similar histograms. Compared to the SVK data, the three RCM simulations underestimate the magnitude of the regional shape parameter (more negative). Only HE50 has a larger regional shape parameter compared to the SVK data. Considering both parameters the spatial resolution of HE50 and HE25 seems to be insufficient to resolve 1 h extreme precipitation.

For daily extreme precipitation, all RCM simulations overestimate the area average μ_x and consequently the 10 year event. HE8 is closest to the area average μ_x of the observations. The

largest spread in the estimates for the 10 year event of HE8 in Figure 4 is due to the wide distribution of μ_x. All RCM simulations seem to reproduce the shape parameter of the observational datasets reasonably well. HE8, HE12 and HE25 produce similar regional shape parameters that underestimate slightly the regional shape parameter of the observations. HE50 slightly overestimates the regional shape parameter.

The two observational datasets produce almost identical regional shape parameters and area average of μ_x. However, the spread and form of the distributions for μ_x differ which can also be derived from the boxplots in Figure 4.

FIGURE 5

Some of the differences between HE outputs at different spatial resolutions might be explained by differences in convective precipitation. The large scale and convective precipitation outputs of HE12 and HE50 have been analysed to get an insight on the relevance of convective precipitation at different resolutions. The approach used as well as a detailed description of the outputs can be found in Appendix A. Overall the results show for both simulations a considerably larger proportion of convective precipitation in summer compared to winter for all exceedance probabilities and a higher percentage of convective precipitation in HE50 for all seasons and temporal aggregations compared to HE12. Higher differences between the convective precipitation in HE12 and HE50 are obtained for the summer season. This is in agreement with the fact that with higher spatial resolution a larger part of total precipitation is resolved in summer and hence the importance of the parameterised convective precipitation decreases (see e.g. Prein et al. 2015a, Prein et al. 2013b).

4.1.3. Spatial pattern

Figure 6 shows the percent variation from the spatial average for the 10 year event for 1 h and 24 h temporal aggregation, and for mean annual precipitation obtained from observations and RCM simulations. CGD is used here to represent the observed pattern over Denmark. The observed mean annual precipitation is between 10 % and 30 % higher on the West Coast of Jutland compared to the spatial average while it is between 0 % and 10 % lower on Zealand (see location of Jutland and Zealand in Figure 1). As in Fig. 5, the outputs from the other six RCM simulations are not included in Fig. 6 for clarity purposes.

HE8, HE12 and HE25 show approximately the same relative spatial pattern as CGD but the spatial pattern of HE8 comes closest to the pattern of CGD followed by HE12. HE50 fails to reproduce the observed spatial pattern. This could be partly caused by the fact that due to the relatively low spatial resolution of this model a large number of grid cells cover both land and sea. Nonetheless, it should be noted that differences in percent variation of the annual mean can still be observed when comparing only grid cells that are 100 % on land, e.g. land grid cells over North and South Jutland. Contrary to CGD, HE50 and to some extent HE25 show highest mean annual precipitation on the coast of North West Jutland. This result challenges the expectation that precipitation properties at scales of around hundred kilometers such as the mean precipitation over the different regions in Denmark are well represented by RCMs across spatial resolutions.

HE8 differs from the other RCM simulations in spatial model domain and spatial resolution. Both could contribute to a more accurate reproduction of the spatial pattern. It is not possible to conclude on which factor dominates the absolute differences in the spatial pattern of mean annual precipitation between HE8 and the other RCM simulations. However, HE12, HE25 and HE50 show that the absolute values of the spatial pattern depend on the spatial resolution.

FIGURE 6

For the 10 year return period at 1h resolution the pattern by HE8 differs from the patterns by HE12 and HE25. Both HE12 and HE25 result in over-average extremes in North West Jutland and East Zealand. It seems that HE12 shows a resolved version of HE25. Conversely, HE8 shows above average extremes spread over Jutland and below average extremes on Zealand. The pattern shown by HE50 differs from the one shown by the other RCM simulations.

At 24 h resolution, the observations show positive deviations (between +10% and +30%) from the spatial average in Central Jutland, North Jutland and North Zealand. The spatial pattern obtained from the RCM simulations depends on the spatial resolution. HE8 agrees with the observations in the positive deviations from the spatial average in Central Jutland but it overestimates the magnitude and the spatial extent of the variation. Further, it does not reproduce the positive deviation band across North Jutland and North Zealand.

HE12 shows positive deviations from the spatial average in Central Jutland, North West Jutland and North Zealand. However, it shows a higher deviation from the spatial average for large parts of Jutland and does not produce the same magnitude of positive deviation in North Jutland and North Zealand compared to the observation dataset. HE25 shows a comparable spatial pattern to HE12. HE50 also shows some similarities to the patterns obtained for HE12 and HE25.

For both 1 and 24 h, the different spatial domains used in HE8 compared to HE12 and HE25 may explain some of the differences in the spatial pattern. However, as suggested from the comparison of the spatial pattern of mean annual precipitation, differences in the spatial pattern also originate from the difference in spatial resolution. Further investigations into the significance and origin of differences in the spatial pattern are needed.

The spatial pattern was also analysed for the 2 year return period (results not shown). For all RCM simulations similar spatial patterns were obtained for the 2 year return period compared to the spatial pattern of the 10 year return period.

4.2. Changes from present to future

The previous section shows that the representation of extreme precipitation at different temporal aggregation partly depends on the spatial resolution of the RCM. This section focuses on the changes projected by the different RCM simulations.

4.2.1. Changes in areal average moments

Figure 7 shows the CFs estimated for all temporal aggregations for moments of order 1 to 3. As in Figure 2, the CF for the moments varies depending on the spatial resolution of the RCM.

All HE simulations for both seasons show an increase in the moment of order 1 (i.e. the mean). The highest increase is obtained for HE8 in summer (CF equal to 1.15) and the lowest is obtained for HE25 in summer (CF equal to 1.02). HE8, HE12 and HE50 lead to higher CFs for summer compared to winter, while the opposite is true for HE25. For illustration purposes the magnitude of these relative changes (the CFs) have been compared with the value of the moment of order 1. For example, in summer the values of HE8 are 0.069 mm/h in the control period and 0.080 mm/h in the future (absolute change of approximately 0.01 mm/h), while in winter HE8 leads to 0.096 mm/h in the control period and 0.101 mm/h in the future (absolute change of approximately 0.005mm/h)

All the HE simulations point to an increase in moments of order 2 and 3 for both seasons, except HE8 for the moment of order 3 in winter for temporal aggregations of 24 and 48h. For both the moments of order 2 and 3, the CFs for summer are in all cases larger than for winter. In addition, the difference between the RCM simulations is larger for summer than winter. The larger changes obtained for summer compared to winter can be illustrated using the absolute values for the control

and the future period. For example, for HE8 the CF obtained for winter for the moment of order 2 points to a change from 0.12 mm^2/h to 0.13 mm^2/h at 1 h temporal aggregation, and from 21.75 mm^2/day to 23.02 mm^2/day at 24 h temporal aggregation, while for summer the change is from 0.24 mm^2/h to 0.46 mm^2/h at 1 h temporal aggregation and 22.5 mm^2/day to 39.7 mm^2/day at 24 h temporal aggregation.

The largest CFs are obtained for HE8 in summer for the moment of order 3. For all HE simulations, higher CFs are obtained for the moments of order 3 than those of order 2, especially for summer. It must be noted that the moment of order 3 is highly dependent on single high precipitation events in the time series. Large values of high order moments are an indication of high values of extreme precipitation. Hence, a larger change in the moment of order 3 points towards a larger increase in extreme precipitation compared to the mean.

For the moments of order 2 and 3, in winter most RCM simulations show similar CFs for all temporal aggregations while in summer all the RCM simulations show lower CFs for higher temporal aggregations. In fact, in winter some RCM simulations show larger changes at higher temporal aggregations.

In summer, in general higher CFs are obtained for higher spatial resolution, i.e. the highest CFs are obtained for HE8 followed by HE12, HE25, and HE50. In winter, there is no clear relation with the spatial resolution of the RCM.

The difference between the CFs obtained for HE8, HN8, WN8 and WE8 are similar to the differences obtained between HE at 8, 12, 25 and 50 km spatial resolution. The four RCMs at 8 km resolution lead to an increase in the moments of order 1, 2 and 3, except HN8 for the mean in summer. For the moments of order 2 and 3 in winter and all temporal aggregations, the CFs obtained from HN8 and WN8, and HE8 and WE8 are similar, respectively. For the mean in winter,

HE8, WN8 and WE8 lead to virtually the same CF while HN8 leads to a higher CF. In summer and for all three moments and temporal aggregations HE8 leads to the largest CFs followed by WE8, WN8 and HN8. The similarities (in winter and for some moments) between the RCMs driven by the same GCM point towards the importance of the GCM in the magnitude of the CFs for all temporal aggregations. However, additional RCM outputs should be used to assess this further.

FIGURE 7

4.2.2. Areal average and spatial pattern of extreme precipitation changes

Figure 8 shows the CFs of the IDF curves for the 2 and 10 year return period. All the RCM outputs point to an increase of extreme precipitation for all temporal aggregations. In agreement with previous studies (e.g. Kendon *et al.*, 2014; Sunyer *et al.*, 2015) and for all temporal aggregations, larger changes are found for the 10 year return period than for the 2 year return period for all RCM simulations. In addition, a larger spread between the changes estimated from the RCM simulations is found for the 10 year return period.

In general, all the HE simulations agree on an increase in CFs for decreasing temporal aggregation, except for HE50 for temporal aggregations larger than 12 h. HE8 shows the smallest difference between CFs at high and low temporal aggregations. This can also be illustrated by looking at the absolute values. For example, for the 10 year return period, HE8 points towards an increase from 7.65 μm/s to 10.95 μm/s (absolute increase of 3.3 μm/s) at 1 h temporal aggregation, and from 0.64 μm/s to 0.84 μm/s (absolute increase of 0.2 μm/s) at 24 h temporal aggregation. HE50 points to an absolute increase of 1.6 μm/s at 1 h temporal aggregation (from 4.76 μm/s to 6.37 μm/s) and of only 0.06 μm/s at 24 h temporal aggregation (from 0.63 μm/s to 0.69 μm/s).

The CFs obtained depend on the spatial resolution of the RCM. Overall, for temporal aggregations between 3 and 48 h and with the exception of the results for 48 h for the 10 year return period and

HE50, the largest CFs are obtained for HE8 followed by HE12, HE25, and HE50. This relation is not observed for the results at 1 h resolution as also shown in Figure 9

The CFs obtained for HE8 are slightly smaller than the CFs estimated by Sørup *et al.* (2015) for 1 h and 24 h temporal aggregation. Sørup *et al.* (2015) used a weather generator to downscale HE8. Sunyer *et al.* (2015) also compared the CFs estimated from the ENSEMBLES project at a spatial resolution of 25 km at 1 and 24 h temporal aggregations. As in this study, they obtained higher CFs at 1 h than at 24 h temporal aggregations. These results are also in agreement with the higher CFs found for short duration in Zheng *et al*. (2015) based on observed annual maximum values for Sydney.

As in the case of extreme events for the current period, the CFs obtained from the other three RCMs at 8 km resolution vary considerably. WN8 and WE8 lead to overall similar results. HN8 shows similar CF for all temporal aggregations. The comparison of these three RCMs at 8 km resolution with the HE simulations at different spatial resolutions point towards slightly larger differences between the CFs obtained from different RCM-GCM simulations than from different spatial resolutions of the RCM.

FIGURE 8

Figure 9 shows boxplots of the magnitude and spatial variation of the CFs for the 10 year return period at 1 and 24 h temporal aggregations. Different spatial resolutions and different RCMs lead to different magnitudes and spatial variations of CFs for both temporal aggregations. As in Figure 4, the differences between the HE simulations are slightly smaller than within the 8 km group (HN8, WE8, WN8). For 1 h temporal aggregation, the magnitude of the CFs does not show any clear relation with the spatial resolution of the HE simulations. On the contrary, the CFs for 24 h show a general decrease for decreasing spatial resolution of the HE model. Apart from WE8 for 24 h, the

spatial variation of the all the CFs increases with higher spatial resolution. These tendencies are different from those obtained for the 10 year event estimates in Figure 4.

The comparison of the year-to-year variation in the HE models using the Wilcoxon Rank Sum show that the median of the CFs obtained from the RCM simulations are significantly different, except for HE12 and HE25 at 1 h resolution.

As discussed as part of the analysis of the extreme precipitation in the control period, convective permitting high resolution RCM outputs might be needed for the analysis of high temporal resolution extreme events. The limitations of coarse resolution models with parameterized convection to reproduce hourly extremes indicate that the change factors are doubtful. Several studies have shown that models with parameterised precipitation show a different response in relation to sub-daily extreme precipitation compared to convection permitting models (e.g. Kendon *et al*. 2014).

FIGURE 9

Figure 10 shows the spatial pattern of CFs for annual mean precipitation and the 10 year event of 1 and 24 h temporal aggregation. The spatial pattern is shown as the percent deviation from the area averaged CF similar to the results shown in Figure 6. As in Fig. 6, the outputs from the other six RCM simulations are not included in Fig. 10 for clarity purposes. All RCM simulations project changes in the spatial pattern of the 10 year event as the comparison of Fig. 6 and Fig. 10 shows.

In the case of the mean annual precipitation, even though all RCM simulations show recognizable and well defined spatial patterns of projected changes, the RCM simulations do not agree on the spatial pattern. The same is observed in the case of extreme precipitation. The RCM simulations also show recognizable and well defined spatial patterns but the patterns differ across the

simulations. In addition, for the same RCM the patterns also differ slightly between the hourly and daily resolutions.

FIGURE 10

5. Conclusion

This study has analysed the performance and projected changes of HIRHAM-ECEARTH RCM as well as six additional RCM outputs (three models from RiskChange at 8 km resolution and three models from ENSEMBLES at 25 km resolution) for extreme precipitation over Denmark at different spatial and temporal aggregations. The temporal aggregations investigated range from 1 to 48h and spatial resolutions from 8 to 50 km. The performance and the projected changes were evaluated for non-central moments of order 1 to 3 and for 2 and 10 year event estimates.

The RCM simulations at higher spatial resolution (8km and 12km, namely HE8 and HE12) are more consistent across all temporal aggregations in the representation of standardised high order moments (i.e. similar over or underestimation for all temporal aggregations). The RCM simulations at lower spatial resolution (25 km and 50 km, namely HE25 and HE50) perform similarly to the higher spatial resolution RCM simulations for high temporal aggregations (> 12h) but worse than the higher spatial resolution RCM simulations for low temporal aggregation.

The performance of the area averaged daily extreme precipitation over Denmark is similar for all RCM simulations at different spatial resolutions. On the contrary, the performance of the RCM simulations differs for hourly extreme precipitation. HE12 and HE25 are closest to the observational dataset. HE8 overestimates and HE50 underestimates hourly extreme precipitation. The HE50 results show that a spatial resolution of 50 km is unsuitable to reproduce hourly extreme precipitation.

The comparison of the shape parameter of the Generalised Pareto Distribution showed that the HIRHAM-ECEARTH model produces more skewed hourly extreme value distributions compared to the observational dataset, except for HE50. The RCM simulations at higher spatial resolutions (HE8 and HE12) seem to overestimate hourly extreme precipitation. In accordance with previous studies this could be an effect caused by the fact that these RCM simulations are in the grey zone. In future research, statistical downscaling methods could be investigated to address unrealistic extreme precipitation results of RCM simulations in the grey zone in the absence of convection resolving RCM simulations.

The biases in the spatial pattern of extreme precipitation change across temporal and spatial resolution. In addition, the difference in model domain may also contribute to differences in the spatial pattern. Further investigations into the significance and origin of differences in the spatial patterns of RCM simulations are needed.

Overall the results of the performance of the RCM simulations point towards the need for high spatial resolution to obtain a better representation of sub-daily extreme precipitation. The RCM simulations at high spatial resolution represent extreme events and high order moments better. However, it should be noted that all RCM simulations are significantly different from the observations according to the Wilcoxon Rank Sum test and that they do not reproduce the observed spatial pattern.

The changes projected by the RCM simulations also depend on the spatial resolution. The RCM simulations agree on a higher increase in extreme precipitation and summer moments for decreasing temporal aggregation but disagree on the magnitude and spatial pattern of the change. The area averaged change factors of the 10 year event over Denmark range between 1.35 and 1.47 for hourly extreme precipitation and between 1.1 and 1.37 for daily extreme precipitation.

Overall, the comparison of the results from the HE models and the different RCM-GCM combinations at the same spatial resolution (RiskChange models at 8 km spatial resolution and ENSEMBLES models at 25 km resolution) show that the differences between the HE simulations are slightly smaller than within the 8 km group (HN8, WE8, WN8) and 25 km group (HEc25, HB25, REc25). This indicates that differences due to spatial resolution are similar to differences caused by different RCM-GCM combinations

Higher CFs in extreme precipitation and summer moments are obtained for higher spatial resolution RCM simulations, i.e. the same RCM at different spatial resolution leads to different changes. This points to possible invalidity of the basic assumption in many statistical downscaling methods that one can apply the change estimated at large scale for higher resolution scales. Additionally, we can conclude that there is a need for high-temporal resolution RCMs for projecting changes in sub-daily extreme precipitation because the change factors differ for different temporal aggregations. Consequently, RCMs at the daily scale are not sufficient for estimation of changes at the hourly scale.

Appendix A

The approach used to analyse and compare the large scale and convective precipitation outputs from HE12 and HE50 is based on a comparison of the empirical cumulative distribution function (ECDF) of the large scale precipitation, convective precipitation and total precipitation (sum of large scale and convective precipitation). The ECDFs are estimated for 1 and 24h temporal aggregation and for winter and summer seasons. The steps followed for each temporal aggregation and seasons are described below:

1. For each grid point, estimate the percentage of convective and large scale precipitation for each precipitation value (wet hours, threshold used to defined wet hours is 0.1 mm/h) in the time series of total precipitation.
2. Estimate the ECDF for wet hours or days in the time series of total precipitation. The quantile interval used to estimate the ECDF is 0.02.
3. For each quantile, find the average percentage of convective and large scale precipitation using the values estimated in step 1.
4. Average over all grids to estimate the percentage of convective and large scale precipitation for each quantile over Denmark.

Figure A1 shows the ECDF of total precipitation and for each quantile the proportion of large scale and convective precipitation for both HE12 and HE50. The results for winter for both 1 h and 24 h show approximately the same percentage of convective precipitation for all quantiles for both HE12 and HE50. In average around 8% for 1 h and 6.5% for 24 h of convective precipitation in HE12. HE50 leads to slightly larger values, in average 10% for both temporal aggregations.

The percentage of convective precipitation is larger in summer than in winter for both HE12 and HE50. As in the case of winter, HE50 has a higher percentage of convective precipitation. For both 1 h and 24 h, there is a slight increase in the percentage of convective precipitation for higher quantiles. For example, for HE12 the percentage of convective precipitation in the 0.5 quantile is 23% while for the 0.98 quantile is 29% for 1 h temporal aggregation. For HE50 and 1 h temporal aggregation, the percentage of convective precipitation for 0.5 is 26% and for 0.98 is 37%. The higher percentage of convective precipitation in summer and for high quantiles was expected as there are more convective storms in summer (i.e. a large part of high precipitation events in summer are caused by convective precipitation).

One important result from this comparison is the higher percentage of convective precipitation in HE50 for all seasons and temporal aggregations (slightly higher differences in summer). This is in agreement with the fact that with higher model resolution a higher part of total precipitation is resolved and hence the importance of the parameterised convective precipitation decreases (see e.g. Prein et al. 2015a, Prein et al. 2013b).

FIGURE A1

Acknowledgements

This work was carried out within the RiskChange project which is supported by the Danish Council for Strategic Research, Contract 10-093894. The authors also thank the Danish Meteorological Institute and Ole Bøssing Christensen and Cathrine Fox Maule who kindly provided the HIRHAM5 data at 1h resolution and at 12 and 50 km spatial resolution.

References

Arnbjerg-Nielsen K, Willems P, Olsson J, Beecham S, Pathirana A, Bülow Gregersen I, Madsen H, Nguyen V-T-V. 2013. Impacts of climate change on rainfall extremes and urban drainage systems: a review. *Water science and technology*. IWA Publishing **68**(1): 16–28. DOI: 10.2166/wst.2013.251.

Ban, N, Schmidli, J, Schär, C. 2014. Evaluation of the convection-resolving regional climate modeling approach in decade-long simulations, *Journal of Geophysical Research: Atmospheres*, **119** (13), 7889–7907. DOI: 10.1002/2014JD021478

Ban, N, Schmidli, J, Schär, C. 2015. Heavy precipitation in a changing climate: Does short-term summer precipitation increase faster? *Geophysical Research Letter* **42**(4): 1165–1172. DOI: 10.1002/2014GL062588

Boberg F, Berg P, Thejll P, Gutowski WJ, Christensen JH. 2010. Improved confidence in climate change projections of precipitation further evaluated using daily statistics from ENSEMBLES models. *Climate Dynamics* **35**: 1509–1520. DOI: 10.1007/s00382-009-0683-8.

Brandt M. 2010. *ECEARTH*. Available at: http://ecearth.knmi.nl/EC-Earth_model_documentation.pdf (Accessed 07.07.2015).

Chan SC, Kendon EJ, Fowler HJ, Blenkinsop S, Roberts NM. 2014a. Projected increases in summer and winter UK sub-daily precipitation extremes from high-resolution regional climate models. *Environmental Research Letters* **9**(8): 084019. DOI: 10.1088/1748-9326/9/8/084019.

Chan SC, Kendon EJ, Fowler HJ, Blenkinsop S, Roberts NM, Ferro CAT. 2014b. The Value of High-Resolution Met Office Regional Climate Models in the Simulation of Multihourly

Precipitation Extremes. *Journal of Climate* **27**(16): 6155–6174. DOI: 10.1275/JCLI-D-13-00723.1.

Chen CT, and Knutson T. 2008. On the Verification and Comparison of Extreme Rainfall Indices from Climate Models, *Journal of Climate* **21**: 1605–1621, DOI:10.1275/2007JCLI1494.1.

Christensen JH, Christensen OB. 2003. Climate modelling: Severe summertime flooding in Europe. *Nature* **421**: 805–806. DOI: 10.1038/421805a.

Christensen OB, Drews M, Dethloff K, Ketelsen K, Hebestadt I, Rinke A. 2007. *Technical report 06-17 The HIRHAM Regional Climate Model Version 5 (β)*. Copenhagen.

Fosser G, Khodayar S, Berg P. 2014. Benefit of convection permitting climate model simulations in the representation of convective precipitation. *Climate Dynamics* **44**: 45-60. DOI: 10.1007/s00382-014-2242-1

Fowler A., Hennessy K. 1995. Potential impacts of global warming on the frequency and magnitude of heavy precipitation. *Natural Hazards* **12**: 283–303. DOI: 10.1007/BF00613412.

Fowler HJ, Ekström M, Blenkinsop S, Smith a. P. 2007. Estimating change in extreme European precipitation using a multimodel ensemble. *Journal of Geophysical Research* **122**: D18104. DOI: 10.1029/2007JD008619.

Fox Maule C, Mayer S, Sobolowski S, Christensen OB. 2014. Background information on the RiskChange simulations by BCCR and DMI. Danish Climate Centre Report 14-05, DMI.

Giorgi F, Gutowski WJ.2015. Regional Dynamical Downscaling and the CORDEX Initiative. *Annu. Rev. Environ. Resour.* **40**:467–90. DOI: 10.1146/annurev-environ-102014-021217

Goodison BE, Louie PYT, Yang, D. 1998. *WMO Solid Precipitation Measurement Intercomparison: Final Report, Report No. 67.* WMO / TD No. 872.

Gregersen IB, Sørup HJD, Madsen H, Rosbjerg D, Mikkelsen PS, Arnbjerg-Nielsen K. 2013. Assessing future climatic changes of rainfall extremes at small spatio-temporal scales. *Climatic Change* **128**(3-4): 783–797. DOI: 10.1007/s10584-012-0669-0.

Grell GA, Freitas SR. 2013. A scale and aerosol aware stochastic convective parameterization for weather and air quality modeling. *Atmos. Chem. Phys. Discuss*. **14**: 5233-5250. DOI:10.5194/acp-14-5233-2014.

Gupta VK, Waymire EC. 1993. A statistical analysis of mesoscale rainfall as a random cascade. Journal of Applied Meteorology and Climatology **32**: 251–267. DOI: 10.1275/1520-0450(1993)032<0251:ASAOMR>2.0.CO;2.

Hanel M, Buishand TA. 2010. On the value of hourly precipitation extremes in regional climate model simulations. *Journal of Hydrology* **393**: 265–273. DOI: 10.1016/j.jhydrol.2010.08.024.

Hosking JRM, Wallis JR. 1993. Some statistics useful in regional frequency analysis. *Water Resources Research* **29**(2): 271–281. DOI: 10.1029/92WR01980.

IPCC. 2012. *Managing the Risks of Extreme Events and Disasters to Advance Climate Change Adaptation. A Special Report of Working Groups I and II of the Intergovernmental Panel on Climate Change*. *Managing the Risks of Extreme Events and Disasters to Advance Climate Change Adaptation*. Cambridge University Press: Cambridge, UK, and New York, NY, USA. DOI: 10.1017/CBO9781239177245.

Jacob D, Petersen J, Eggert B, Alias A, Christensen OB, Bouwer LM, Braun A, Colette A, Déqué M, Georgievski G, Georgopoulou E, Gobiet A, Menut L, Nikulin G, Haensler A,

Hempelmann N, Jones C, Keuler K, Kovats S, Kröner N, Kotlarski S, Kriegsmann A, Martin E, Meijgaard E, Moseley C, Pfeifer S, Preuschmann S, Radermacher C, Radtke K, Rechid D, Rounsevell M, Samuelsson P, Somot S, Soussana J-F, Teichmann C, Valentini R, Vautard R, Weber B, Yiou P. 2013. EURO-CORDEX: new high-resolution climate change projections for European impact research. *Regional Environmental Change* **14**(2): 563–578. DOI: 10.1007/s10123-013-0499-2.

Jørgensen HK, Rosenørn S, Madsen H, Mikkelsen PS, 1998. Quality control of rain data used for urban runoff systems. *Water Science and Technology* **37**(12): 123-120. DOI: 10.1016/S0273-1223(98)00323-0

Kendon EJ, Roberts NM, Fowler HJ, Roberts MJ, Chan SC, Senior CA. 2014. Heavier summer downpours with climate change revealed by weather forecast resolution model. *Nature Climate Change*. Nature Publishing Group **4**(7): 570–576. DOI: 10.1038/nclimate2258.

Kjellström E, Boberg F, Castro M, Christensen JH, Nikulin G, Sanchez E. 2010. Daily and monthly temperature and precipitation statistics as performance indicators for regional climate models. *Climate Research* **44**(2-3): 135–150. DOI: 10.3354/cr00932.

Madsen H, Arnbjerg-Nielsen K, Mikkelsen PS. 2009. Update of regional intensity-duration frequency curves in Denmark: Tendency towards increased storm intensities. *Atmospheric Research* **92**(3): 343–349. DOI: 10.1016/j.atmosres.2009.01.013.

Madsen H, Mikkelsen PS, Rosbjerg D, Harremoës P. 2002. Regional estimation of rainfall intensity-duration-frequency curves using generalized least squares regression of partial duration series statistics. *Water Resources Research* **38**: 1239. DOI: 10.1029/2001WR001225.

Maraun D, Wetterhall F, Ireson AM, Chandler RE, Kendon EJ, Widmann M, Brienen S, Rust HW, Sauter T, Venema VKC, Chun KP, Goodess CM, Jones RG, Onof C, Vrac M, Thiele-Eich I. 2010. Precipitation downscaling under climate change. Recent developments to bridge the gap between dynamical models and the end user. *Reviews of Geophysics* **48**(3): RG3003. DOI: 10.1029/2009RG000314.

Mayer S, Maule CF, Sobolowski S, Christensen OB, Danielsen Sørup HJ, Sunyer MA, Arnbjerg-Nielsen K, Barstad I. 2015. Identifying added value in high-resolution climate simulations over Scandinavia. *Tellus A* **67**: 1–36. DOI: 10.3402/tellusa.v67.24941.

McMillan H, Krueger T, Freer J. 2012. Benchmarking observational Uncertainties of hydrology: rainfall, river discharge, and water quality. *Hydrological Processes* **26**(26): 4078–4121. DOI: 10.1002/hyp.9384

Molnar P, Burlando P. 2005. Preservation of rainfall properties in stochastic disaggregation by a simple random cascade model. *Atmospheric Research* **77**: 137–151. DOI: 10.1016/j.atmosres.2004.10.024.

Moss RH, Edmonds JA, Hibbard KA, Manning MR, Rose SK, van Vuuren DP, Carter TR, Emori S, Kainuma M, Kram T, Meehl GA, Mitchell JFB, Nakicenovic N, Riahi K, Smith SJ, Stouffer RJ, Thomson AM, Weyant JP, Wilbanks TJ. 2010. The next generation of scenarios for climate change research and assessment. *Nature* **463**(7282): 747–56. DOI: 10.1038/nature08823.

Nakićenović N, Alcamo J, Davis J, de Vries B, Fenhann J, Gaffin S, Gregory K, Grübler A, Jung TY, Kram T, Lebre La Rovere E, Michaelis L, Mori S, Morita T, Pepper W, Pitcher H, Price L, Riahi K, Roehrl A, Rogner HH, Sankovski A, Schlesinger M, Shukla P, Smith S, Swart R, van Rooijen S, Victor N, Dadi Z. 2000. Special report on emission scenarios. A special report

of Working Group III for the Intergovernmental Panel on Climate Change. *Cambridge University Press*, New York.

Nguyen V-T-V, Nguyen T-D, Cung A. 2007. A statistical approach to downscaling of sub-daily extreme rainfall processes for climate-related impact studies in urban areas. Water Science and Technology **7**: 183–192, DOI: 10.2166/ws.2007.053.

Onof C, Arnbjerg-Nielsen K. 2009. Quantification of anticipated future changes in high resolution design rainfall for urban areas. *Atmospheric Research* **92**: 350–363. DOI: 10.1016/j.atmosres.2009.01.014.

Over TM, Gupta VK. 1996. A space–time theory of mesoscale rainfall using random cascades. *Journal of Geophysical Research* **101**(D21): 26319– 26331. DOI: 10.1029/96JD02033.

Prein, AF, Gobiet A, Suklitsch M, Truhetz H, Awan NK, Keuler K, Georgievski G. 2013a. Added value of convection permitting seasonal simulations. *Climate Dynamics* **41(9)**: 2655–2677. DOI 10.1007/s00382-013-1744-6

Prein, AF, Holland GJ, Rasmussen RM, Done J, Ikeda K, Clark MP, Liu CH. 2013b. Importance of regional climate model grid spacing for the simulation of heavy precipitation in the Colorado headwaters. *Journal of Climate* **26(13)**: 4848 – 4857. DOI: 10.1175/JCLI-D-12-00727.1

Prein, AF, Gobiet A, Truhetz H, Keuler K, Goergen K, Teichmann C, Fox Maule C, van Meijgaard E, Déqué M, Nikulin G,Vautard R, Colette A, Kjellström E, Jacob D. 2015a. Precipitation in the EURO-CORDEX 0.11º and 0.44 º simulations: high resolution, high benefits?. *Climate Dynamics* **46(1)**: 1 – 30. DOI: 10.1007/s00382-015-2589-y.

Prein, AF, Langhans W, Fosser G, Ferrone A, Ban N, Goergen K, Keller M, Tölle M, Gutjahr O, Feser F, Brisson E, Kollet S, Schmidli J, van Lipzig NPM, Leung R. 2015b. A review on

regional convection-permitting climate modelling: demonstrations, prospects, and challenges. *Reviews of Geophysics*. **53**: 323–361. DOI: 10.1002/2014RG000475

Roeckner E, Bäuml G, Bonaventura L, Brokopf R, Esch M, Giorgetta M, Hagemann S, Kirchner I, Kornblueh L, Rhodin A, Schlese U, Schulzweida U, Tompkins A. 2003. *The atmospheric general circulation model ECHAM5: Part 1: Model description*. MPI for Meteorology.

Scharling M. 2012. *Climate Grid Denmark, Technical Report no 12-10*. Denmark.

Schilling W. 1991. Rainfall data for urban hydrology: what do we need? *Atmospheric Research* **27**(1-3): 5–21. DOI: 10.1016/0169-8095(91)90003-F.

Sunyer MA, Rosbjerg D, Madsen H, Luchner J, Arnbjerg-Nielsen K. 2015. Comparison of different statistical downscaling methods to estimate changes in hourly extreme precipitation using RCM projections from ENSEMBLES. *International Journal of Climatology* **35**: 2528-2539. DOI: 10.1002/joc.4138.

Sunyer MA, Sørup HJD, Christensen OB, Madsen H, Rosbjerg D, Mikkelsen PS, Arnbjerg-Nielsen K. 2013. On the importance of observational data properties when assessing regional climate model performance of extreme precipitation, *Hydrology and Earth System Sciences* **17**: 4323–4337. DOI: 10.5194/hess-17-4323-2013.

Sørup HJD, Christensen OB, Arnbjerg-Nielsen K, Mikkelsen PS. 2015. Downscaling future precipitation extremes to urban hydrology scales using a spatio-temporal Neyman–Scott weather generator. *Hydrology and Earth System Sciences Discussions* **12**(2): 2561–2605. DOI: 10.5194/hessd-12-2561-2015.

Tripathi OP, Dominguez F. 2013. Effects of spatial resolution in the simulation of daily and subdaily precipitation in the southwestern US. *Journal of Geophysical Research: Atmospheres* **128**(14): 7591–7605. DOI: 10.1002/jgrd.50590.

Unden P, Rontu L, Jarvinen H, Lynch P, Calvo J, Cats G, Cuxart J, Eerola K, Fortelius C, Garcia-moya JA, Jones C, Lenderlink G, Mcdonald A, Mcgrath R, Navascues B. 2002. *Hirlam-5 Scientific Documentation*. Norrkoeping, Sweden.

Van der Linden P, Mitchell JFB. 2009. *Ensembles: Climate change and its impacts: Summary of research and results from the ensembles project*. Met Office Hadley Centre, FitzRoy Road, Exeter EX1 3PB, UK.

Weisman ML, Skamarock WC, Klemp JB. 1997. The resolution dependence of explicitly modeled convective systems. *Monthly Weather Review* **125 (4)**: 527–548. DOI: 10.1175/1520-0493(1997)125<0527:TRDOEM>2.0.CO;2

Westra S, Fowler HJ, Evans JP, Alexander L., Berg P, Johnson F, Kendon EJ, Lenderink G, Roberts NM. 2014. Future changes to the intensity and frequency of short-duration extreme rainfall. *Reviews of Geophysics* **52**(3): 522–555. DOI: 10.1002/2014RG000464.

Willems P, Vrac M. 2012. Statistical precipitation downscaling for small-scale hydrological impact investigations of climate change. *Journal of Hydrology* **402**: 193–205. DOI: 10.1016/j.jhydrol.2012.02.030.

Wilson EM. 1990. *Engineering Hydrology*, Macmillan Education Ltd: London, UK.

Yu X, Lee T-Y. 2010. Role of convective parameterization in simulations of a convection band at grey-zone resolutions. *Tellus A* **62A**: 617–632. DOI: 10.1212/j.1600-0870.2010.00470.x.

Zheng F, Westra S, Leonard M. 2015. Opposing local precipitation extremes. *Nature Climate Change* **5**: 389 – 390. DOI: 10.1038/nclimate2579.

List of table captions

Table 1 - Areal Reduction Factors for extreme precipitation to scale from areal to point measurements obtained from to Wilson (1990). Note that ARF for 10 km and 1 h temporal aggregation is not used in this study.

List of figure captions

Figure 1 - Position of the SVK stations included and grid points from CGD, HE8, HE12, HE25, and HE50. The two main regions in Denmark (Jutland and Zealand) are also indicated in the top left map

Figure 2 - Log-log plots of moments 1, 2, and 3 vs. temporal aggregation, log(λ), for the observations and RCM simulations for winter (left) and summer (right) averaged over Denmark. The shaded area represents the minimum and maximum values of all the SVK stations

Figure 3 - IDF curves for 2 and 10 years return periods. ARF have been applied to the RCM simulations to "downscale" the T-year events to point estimates. Shaded area shows the spectrum covered by all the bootstrapping samples from the SVK stations. All the results represent the area average intensity over Denmark. The grey lines represent the RCM-GCM combinations that are not HIRHAM-ECEARTH, the dashed lines are used for the RCMs at 25 km resolution and solid line for the RCMs at 8 km resolution.

Figure 4 - Boxplots of extreme precipitation estimates for all Danish land grid cells for RCM data at different spatial resolutions and observed data products. ARF are applied to transform all gridded data into point data. The lower, centre and upper line of the box indicate the 25th, 50th and 75th

percentile of the data, respectively. The lower and upper ends of the whiskers indicate the 5th and 95th percentile of the data, respectively.

Figure 5 Comparison of parameters of the GPD between the different RCM simulations and observations. 24h statistics: μ_x of the extreme value time series (column 1), k for GPD (column 2); 1h statistics: μ_x of the extreme value time series (column 3), k for GDP (column 4). ARF have been applied to μ_x so that all datasets represent point measurements. The red line indicates the area average. For k, the red line indicates the regional shape parameter.

Figure 6 Percent variation from spatial average, Δ, of the mean annual precipitation (top), 10 year event of 1h extreme precipitation (middle) and 10 year event of 24h extreme precipitation (bottom). The average is calculated from all Danish land grid cells of the respective dataset.

Figure 7 – Average changes over Denmark in the moments q=1, 2, and 3 for different temporal aggregation estimated from the RCM simulations (left: winter, right: summer).

Figure 8 - Changes in IDF curves estimated from the RCM simulations for different durations

Figure 9 - Boxplots of change factors of 10 year precipitation estimates for all Danish land grid cells for RCM data at different spatial resolutions. Left: 1h precipitation. Right: 24h precipitation. The lower, center and upper line of the box indicate the 25th, 50th and 75th percentile of the data, respectively. The lower and upper ends of the whiskers indicate the 5th and 95th percentile of the data, respectively.

Figure 10 - Percent variation from spatial average of CFs, Δ, of mean annual precipitation (top), 10 year event for 1 h extreme precipitation (middle) and 10 year event for 24 h extreme precipitation (bottom).

Figure A1 – ECDF of total precipitation (in black) for HE12 (top) and HE50 (middle), proportion of convective precipitation (dark grey) and large scale precipitation (light grey) for each quantile. Percentage of convective precipitation for HE12 and HE50 for each quantile (bottom)

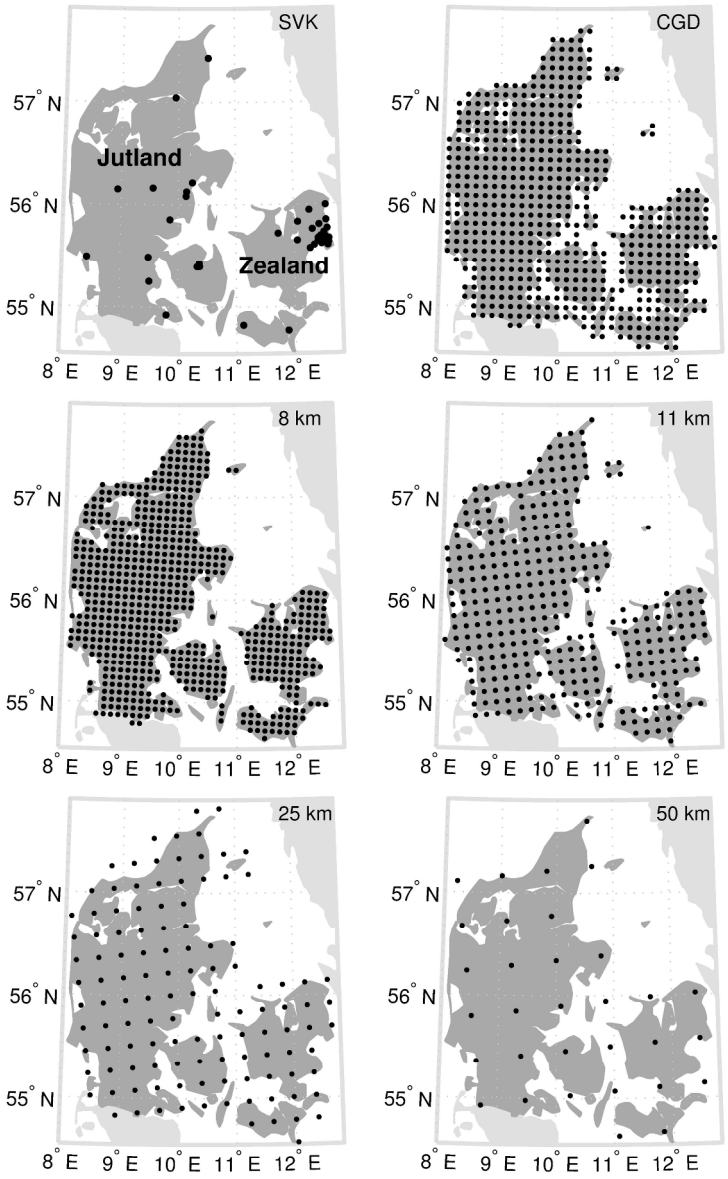

Figure 1 - Position of the SVK stations included and grid points from CGD, HE8, HE12, HE25, and HE50. The two main regions in Denmark (Jutland and Zealand) are also indicated in the top left map
212x323mm (300 x 300 DPI)

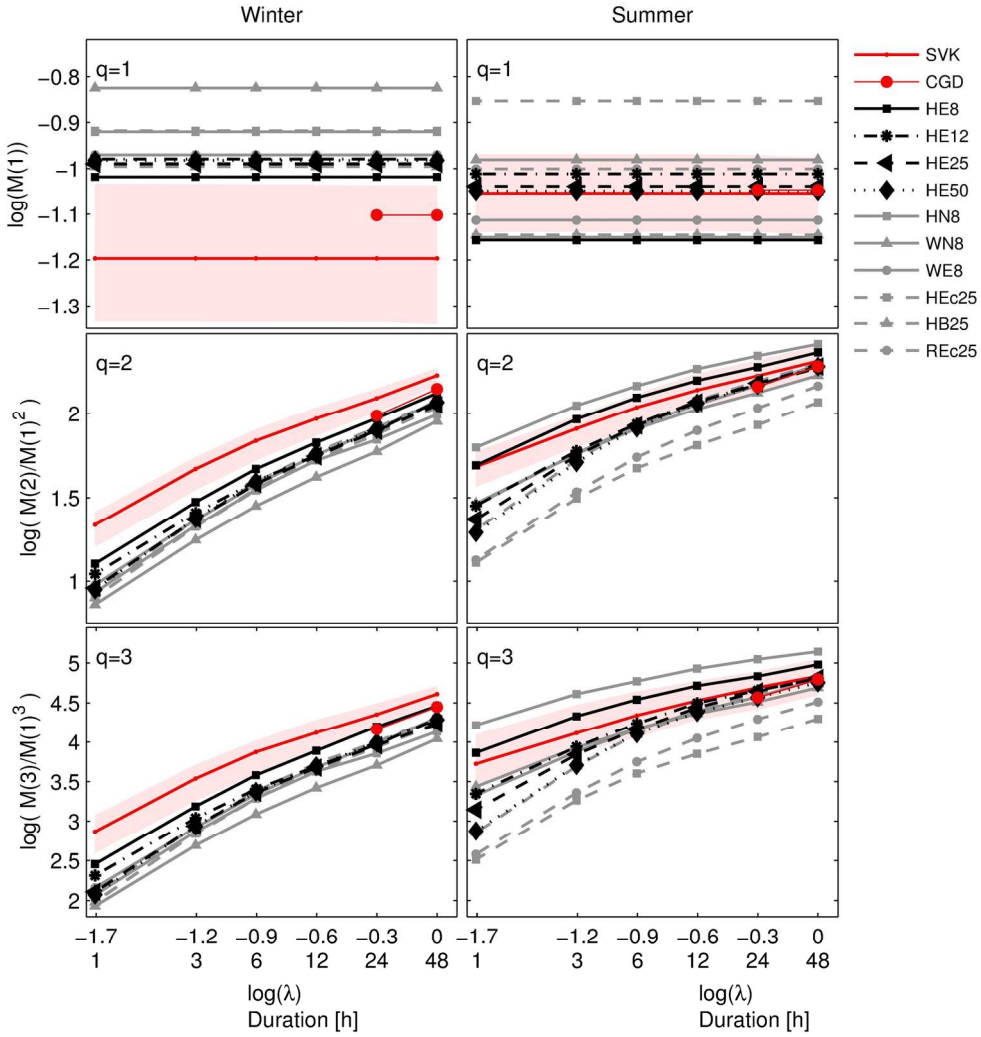

Figure 2 - Log-log plots of moments 1, 2, and 3 vs. temporal aggregation, log(λ), for the observations and RCM simulations for winter (left) and summer (right) averaged over Denmark. The shaded area represents the minimum and maximum values of all the SVK stations
172x180mm (300 x 300 DPI)

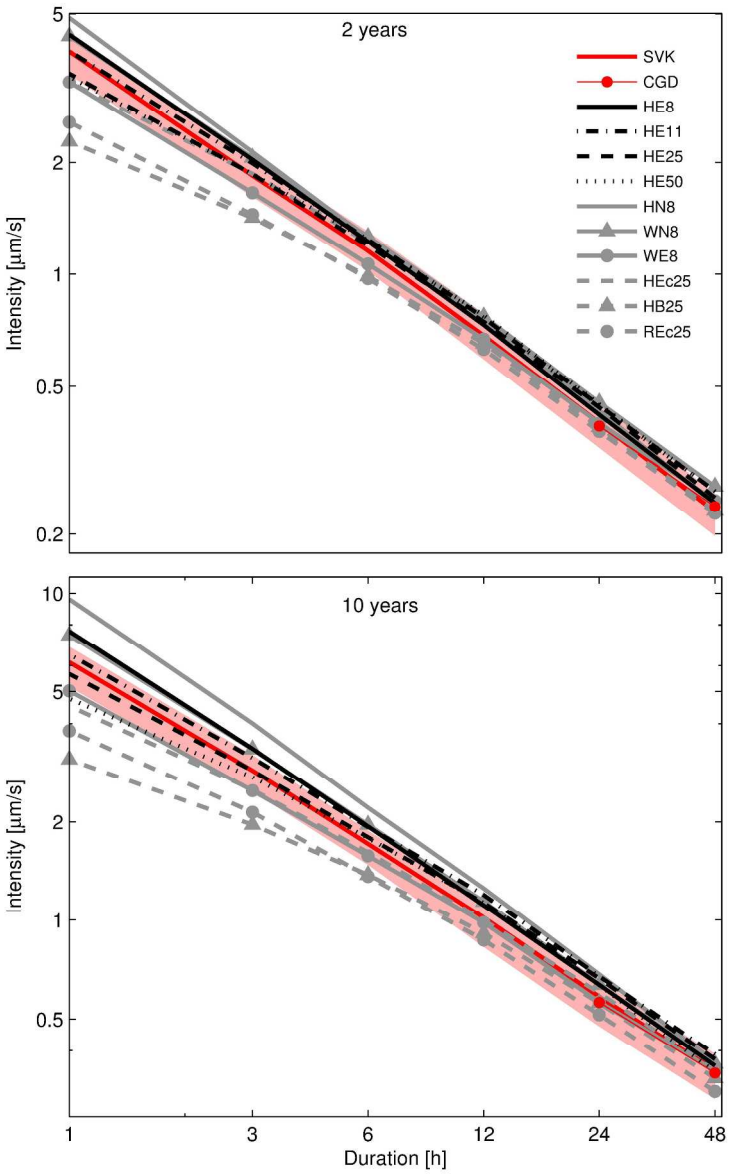

Figure 3 - IDF curves for 2 and 10 years return periods. ARF have been applied to the RCM simulations to "downscale" the T-year events to point estimates. Shaded area shows the spectrum covered by all the bootstrapping samples from the SVK stations. All the results represent the area average intensity over Denmark. The grey lines represent the RCM-GCM combinations that are not HIRHAM-ECEARTH, the dashed lines are used for the RCMs at 25 km resolution and solid line for the RCMs at 8 km resolution.
212x339mm (300 x 300 DPI)

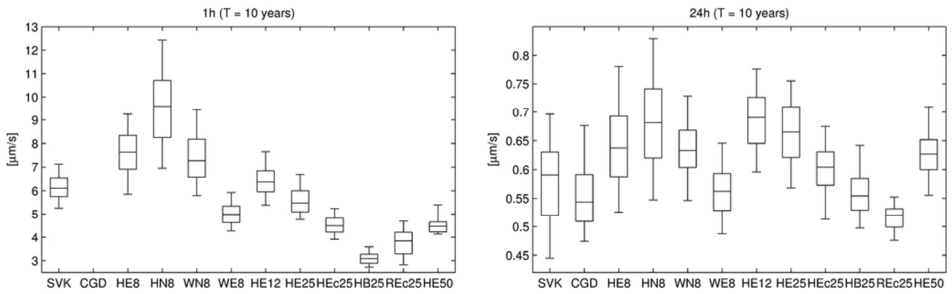

Figure 4 - Boxplots of extreme precipitation estimates for all Danish land grid cells for RCM data at different spatial resolutions and observed data products. ARF are applied to transform all gridded data into point data. The lower, centre and upper line of the box indicate the 25th, 50th and 75th percentile of the data, respectively. The lower and upper ends of the whiskers indicate the 5th and 95th percentile of the data, respectively.
92x29mm (300 x 300 DPI)

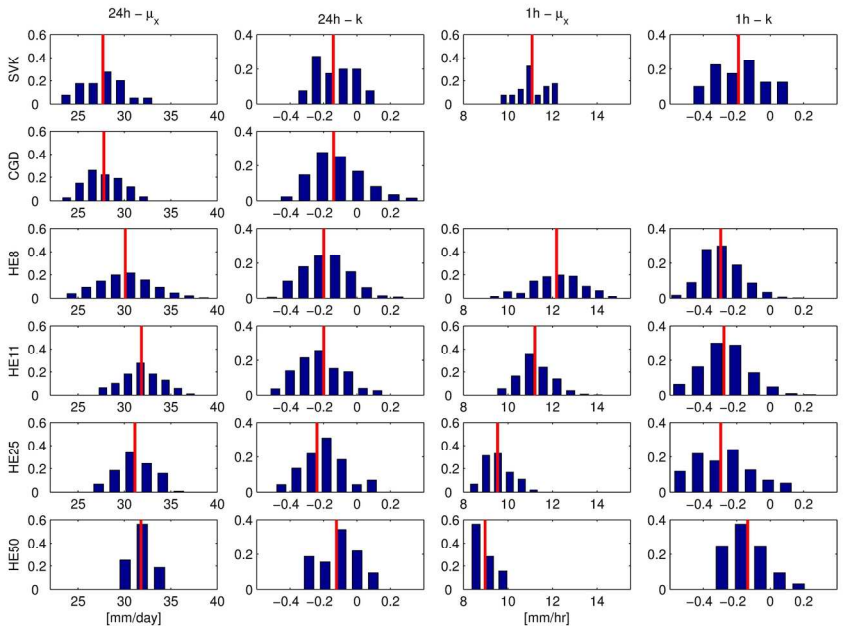

Figure 5 Comparison of parameters of the GPD between the different RCM simulations and observations. 24h statistics: μx of the extreme value time series (column 1), k for GPD (column 2); 1h statistics: μx of the extreme value time series (column 3), k for GDP (column 4). ARF have been applied to μx so that all datasets represent point measurements. The red line indicates the area average. For k, the red line indicates the regional shape parameter.
179x122mm (300 x 300 DPI)

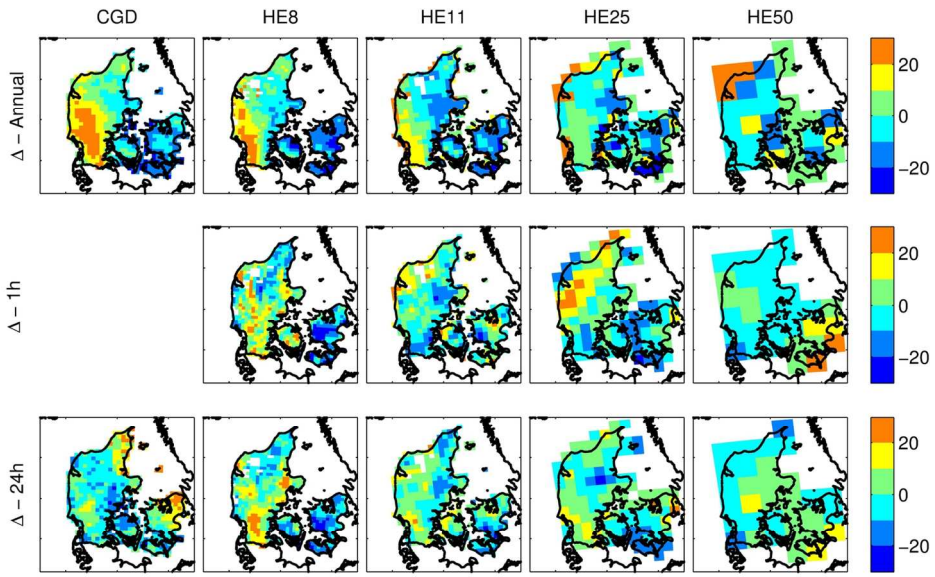

Figure 6 Percent variation from spatial average, Δ, of the mean annual precipitation (top), 10 year event of 1h extreme precipitation (middle) and 10 year event of 24h extreme precipitation (bottom). The average is calculated from all Danish land grid cells of the respective dataset.
144x91mm (300 x 300 DPI)

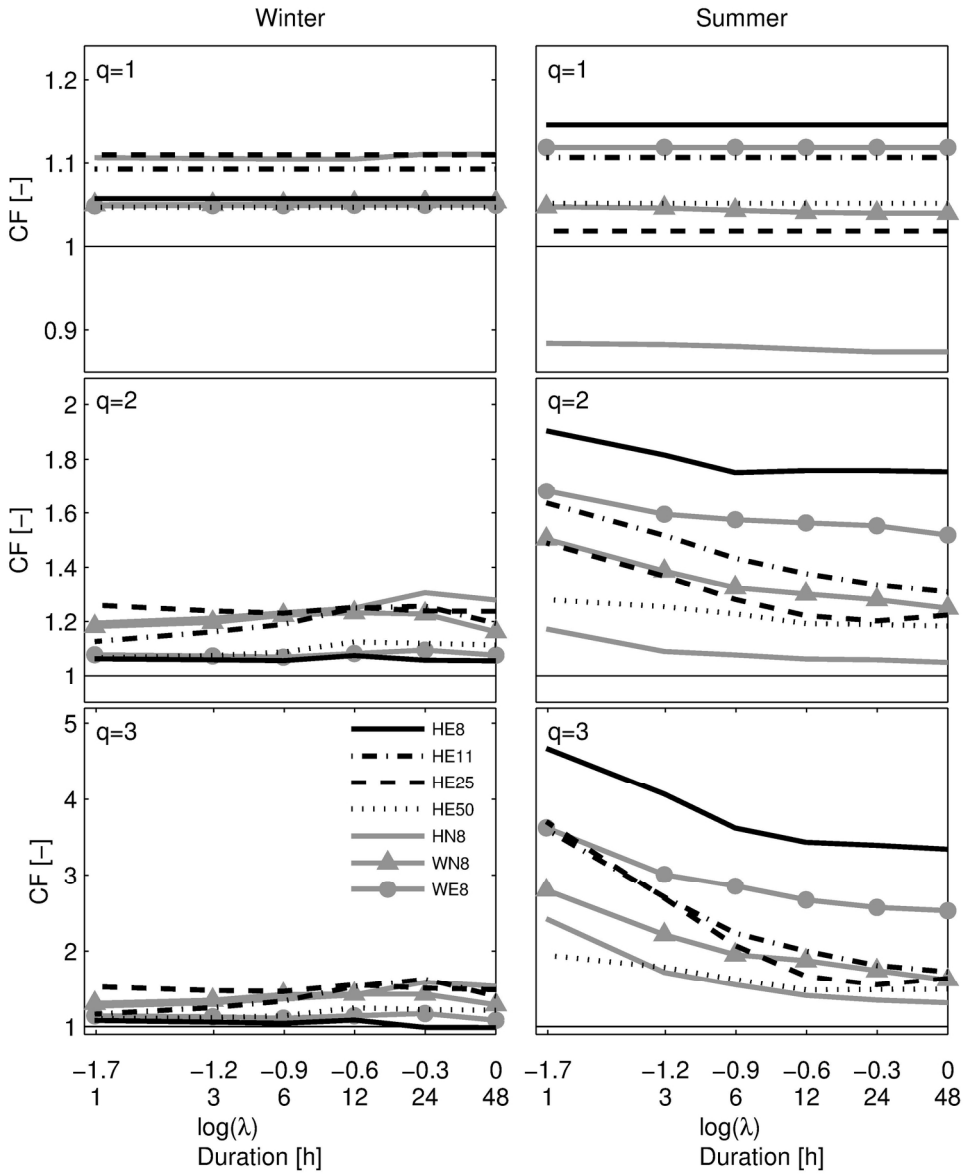

Figure 7 – Average changes over Denmark in the moments q=1, 2, and 3 for different temporal aggregation estimated from the RCM simulations (left: winter, right: summer).
172x203mm (300 x 300 DPI)

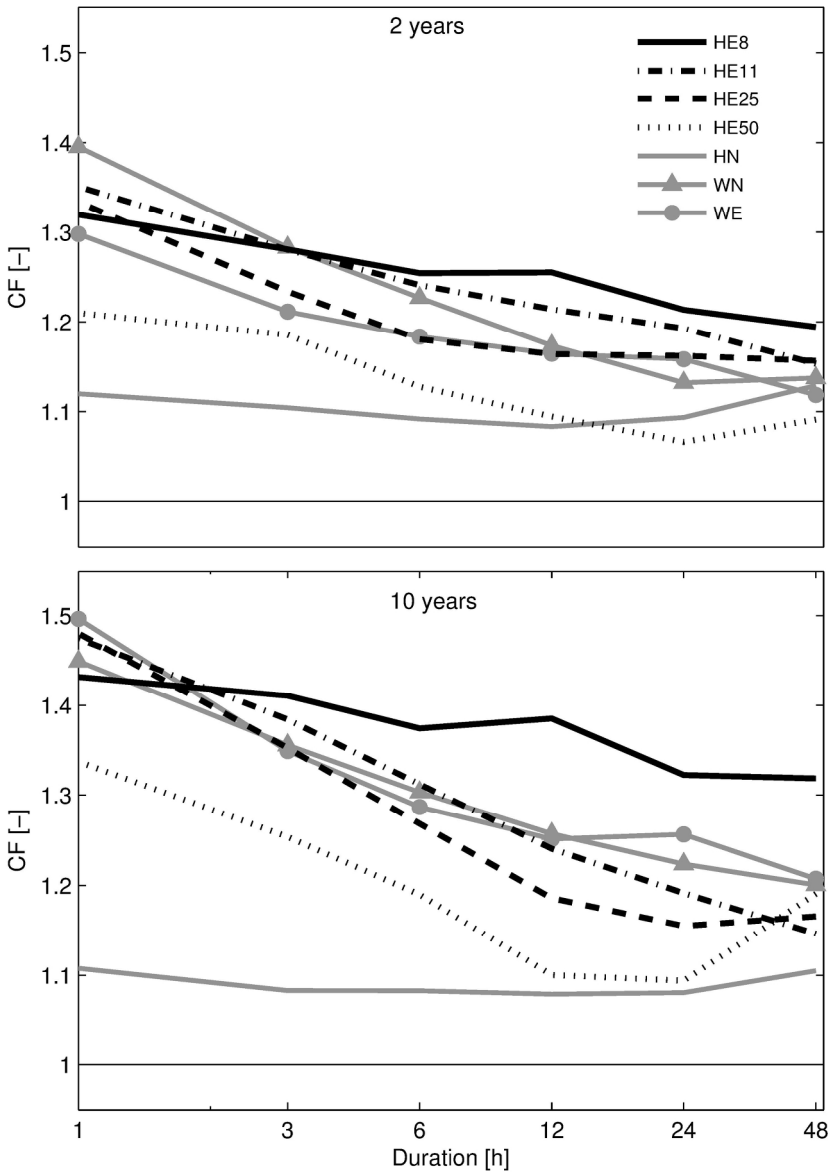

Figure 8 - Changes in IDF curves estimated from the RCM simulations for different durations
185x260mm (300 x 300 DPI)

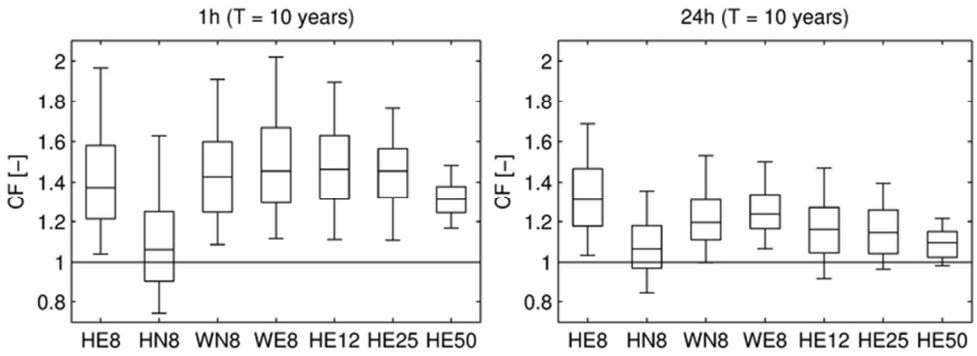

Figure 9 - Boxplots of change factors of 10 year precipitation estimates for all Danish land grid cells for RCM data at different spatial resolutions. Left: 1h precipitation. Right: 24h precipitation. The lower, center and upper line of the box indicate the 25th, 50th and 75th percentile of the data, respectively. The lower and upper ends of the whiskers indicate the 5th and 95th percentile of the data, respectively.
66x25mm (300 x 300 DPI)

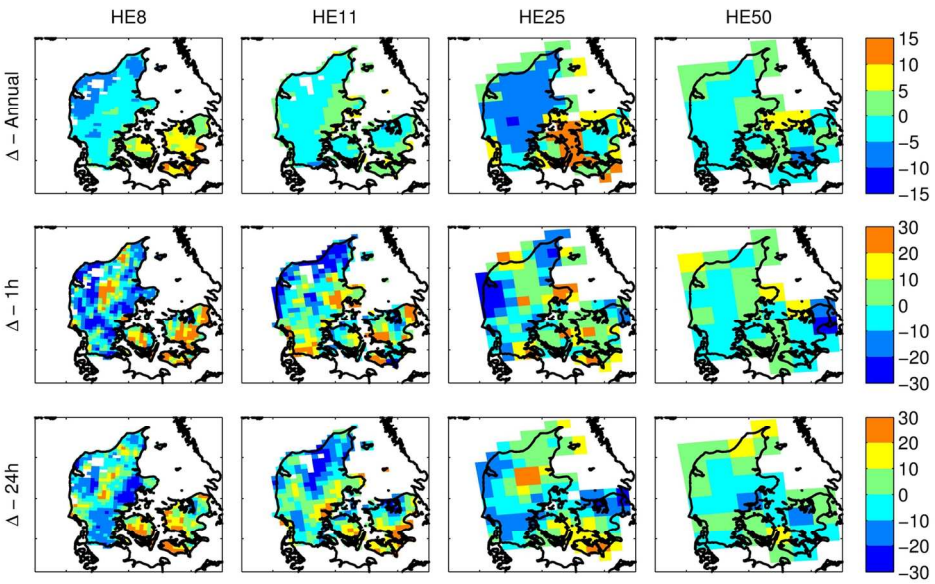

Figure 10 - Percent variation from spatial average of CFs, Δ, of mean annual precipitation (top), 10 year event for 1 h extreme precipitation (middle) and 10 year event for 24 h extreme precipitation (bottom). 144x91mm (300 x 300 DPI)

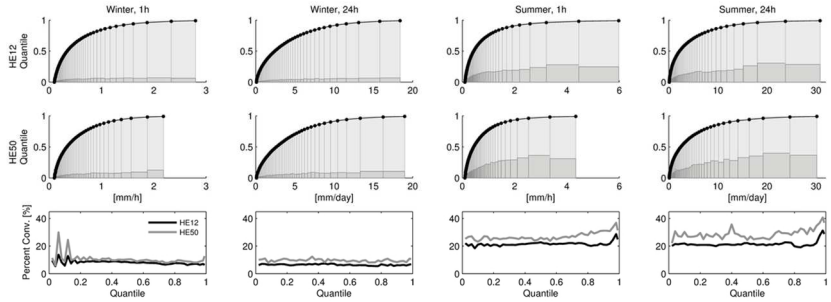

Figure A1 – ECDF of total precipitation (in black) for HE12 (top) and HE50 (middle), proportion of convective precipitation (dark grey) and large scale precipitation (light grey) for each quantile. Percentage of convective precipitation for HE12 and HE50 for each quantile (bottom)
120x38mm (300 x 300 DPI)

Table 1 – Areal Reduction Factors for extreme precipitation to scale from areal to point measurements obtained from to Wilson (1990). Note that ARF for 10 km and 1 h temporal aggregation is not used in this study.

	8km	10km	12km	25km	50km
1h	1.211	1.266	1.279	1.497	1.739
24h	1.052	1.064	1.066	1.104	1.143